

A Fast and Adaptable Algorithm for Optimal Multi-Qubit Pathfinding in Quantum Circuit Compilation

Gary J Mooney^{1,*}

¹*School of Physics, University of Melbourne, VIC, Parkville, 3010, Australia.*

(Dated: May 30, 2024)

Quantum computing has the potential to significantly enhance our ability to simulate and solve complex, classically intractable problems across various fields of research and industry. However, we are currently in the noisy intermediate-scale quantum (NISQ) era, where devices are relatively small and suffer from substantial noise levels, prohibiting large-scale computations. To achieve any quantum advantage in this regime and beyond, it is crucial to minimise the impact of noise from qubit decoherence and two-qubit gates. A direct approach is to improve the optimisation of quantum circuit compilation processes that map circuits onto physical devices, thereby reducing noisy gates and circuit execution times. This work focuses on multi-qubit pathfinding as a critical subroutine within the quantum circuit compilation mapping problem. We introduce an algorithm, modelled using binary integer linear programming, that navigates qubits on quantum hardware optimally with respect to circuit SWAP-gate depth, while also optimising for accumulated gate errors and can be flexibly adapted to various problem modifications. This multi-qubit pathfinding algorithm incorporates considerations for gate-error penalties, SWAP movement constraints, and configurable arrangements of source and target qubit locations and qubit teams. We have benchmarked the algorithm across a variety of quantum hardware layouts, assessing properties such as computational runtimes, solution SWAP depths, and accumulated SWAP-gate error rates. The results demonstrate the algorithm's practical runtimes on current quantum devices and compare its effectiveness across different hardware configurations, providing insights for future quantum hardware design.

I. INTRODUCTION

Quantum computing technology is currently in the Noisy Intermediate-Scale Quantum (NISQ) era. Executing robust algorithms for realistic problem sizes remains challenging due to the significant noise in these devices, predominantly from two-qubit gate error rates and qubit decoherence. This noise limits the number of two-qubit gates that can be applied before the results are obfuscated. To combat these limitations and perform the largest algorithms possible on current quantum hardware, it is crucial to optimise quantum circuits during compilation to NISQ devices. This involves minimising both the circuit execution time and the number of two-qubit gates while prioritising low error rates.

There are two major compilation stages when mapping an arbitrary logical quantum circuit to a target NISQ device. In the first stage, the original gates of the circuit are decomposed into base gates that are directly supported by the device. Typically, the set of possible base gates in a decomposed circuit consists of a two-qubit gate and parameterised single qubit gates. In the second stage of compilation, the logical circuit is mapped to the hardware graph of a NISQ device by representing each logical qubit with a physical one. Implementing a logical two-qubit gate on the device thus requires its corresponding physical qubits to be adjacent to one another. However, due to the limited connectivity of many NISQ-devices, logical qubits in typical quantum circuits need to be frequently relocated to satisfy gate adjacency requirements. The standard approach for qubit relocation is to use sequences of SWAP gates, each constructed from three CNOT gates. Thus, mapping to the hardware graph can lead to a significant overhead in the number of CNOT gates and the CNOT depth of circuits. Optimising the quantum circuit during this stage can alleviate this overhead and significantly reduce the quantum resource requirements.

In this work, we focus on the second major stage of circuit compilation which we refer to as *quantum circuit mapping*. This process involves mapping arbitrary circuits to devices with restricted-connectivity qubit layouts via sequences of SWAP gates. The problem of determining optimal mappings has been shown to be NP-complete, both in cases of minimising the total number of SWAP gates and minimising the SWAP depth (makespan) of the final circuit [1, 2]. A variety of heuristic and optimal approaches to the quantum circuit mapping problem have been introduced in the quantum compilation literature [3, 4]. For example, algorithms based on integer linear programming (ILP) [5], search methods [6–9], boolean satisfiability [10, 11], pseudo-boolean optimisation [12], graph theory [13], machine learning [14], recursive-subcircuit cutting [1], specific architecture tailoring [15], and temporal planning [16–18], are all

* mooneyg@unimelb.edu.au

considered. As the size of quantum devices and circuits increases, optimal quantum circuit mapping quickly becomes intractable, even for relatively small devices of around 10 qubits [10, 11]. Consequently, in practice, optimality is often foregone in favor of applying combinations of heuristic techniques, approximations, or problem simplifications. A common simplification involves splitting the circuit into interaction layers, where each layer contains the maximal number of logical two-qubit interactions that can be processed in parallel [8]. The challenge then reduces to finding a minimal SWAP gate schedule for each interaction layer to route qubits to destinations that facilitate the necessary two-qubit gates. This process can be further reduced to alternating between two main steps [1, 19]. The first step, qubit allocation [20, 21], involves assigning physical qubits on the device hardware graph to satisfy the adjacency requirements of logical qubits in the interaction layer. The second step, multi-qubit pathfinding (MQPF), which is the focus of this paper, routes the logical qubits in the hardware graph to their target assignments using sequences of SWAP operations. Various heuristic and optimal methods exist for addressing the MQPF problem and its variants, including algorithms based on propositional satisfiability (SAT) [22, 23], Pseudo-Boolean Optimisation [24], recursive subcircuit cutting [1], and ILP (independently developed with a distinct approach from ours) [5]. Although each subproblem introduced by simplification—interaction layer SWAP scheduling, qubit allocation, and MQPF—is NP-hard, these simplifications greatly reduce the size of the problems individually, leading to a considerable computational speedup compared to the full quantum circuit compilation problem, which has been shown to be formulatable as a travelling salesman problem on a torus [25].

We present a SWAP-depth optimal MQPF algorithm that achieves practical runtimes on current quantum hardware. The algorithm is modelled using binary integer linear programming (BILP) and initially optimises for the SWAP depth of the circuit as a primary objective, and then optimises for the accumulated SWAP gate error rate as a secondary objective. The algorithm supports multiple teams of qubits, each sharing its own set of destinations, where qubits in a team are indifferent to which of the team’s assigned destinations they reach. Strictly speaking, for K teams of qubits the problem is equivalent to a weighted variant of the parallel $(K+1)$ -coloured token swapping problem, which we discuss in Section IID. However, our algorithm additionally supports the number of destinations for a team being greater than the number of qubits in the team, allowing the qubits to be routed to any subset of destinations. This also enables multiple teams to share the same destination in their destination sets at the same time. Properties of the algorithm’s outputs, such as computational runtimes, solution SWAP depths, and accumulated SWAP gate error rates, were compared and analysed across the variety of device qubit layouts shown in Figure 1.

In Section II, we discuss relevant existing techniques for modelling variations of multi-agent pathfinding problems. In Section III, we formally define the MQPF problem and discuss the steps involved in modelling it using a BILP approach. In Section IV A, we describe the details of the experimental implementation and present the results. In Section V, we conclude with a discussion of the results.

II. TECHNIQUES TOWARD MULTI-QUBIT PATHFINDING

A. Linear Programming

Linear programming is a widely used optimisation method for problems that can be represented as a set of linear constraints with real variables, aimed at maximising or minimising a specified linear cost function, also commonly referred to as the objective function. LP is extensively used to model a broad array of real-world problems, including various scheduling, resource allocation, transportation, and routing problems. The power of this method comes from its capability to find optimal solutions in polynomial time, combined with the flexibility it offers in application—especially when simplifying assumptions are integrated into the model.

The standard form of an LP can be written as

$$\max \mathbf{c} \cdot \mathbf{x}, \tag{1}$$

$$\text{such that } A\mathbf{x} \leq \mathbf{b}, \tag{2}$$

$$\text{and } x_i \geq 0, \tag{3}$$

$$\text{where } x_i \in \mathbb{R}, \quad i = 0, 1, \dots, n, \tag{4}$$

where $\mathbf{c} = (c_1, c_2, \dots, c_n) \in \mathbb{R}^n$ is the coefficient vector of the objective function, $\mathbf{x} = (x_1, x_2, \dots, x_n) \in \mathbb{R}^n$ is the vector of variables to be determined, and $\mathbf{b} = (b_1, b_2, \dots, b_m) \in \mathbb{R}^m$ is the vector of constants defining the upper bounds in the constraints. The constraint matrix A is given by:

$$A = \begin{pmatrix} a_{1,1} & \dots & a_{1,n} \\ \vdots & \ddots & \vdots \\ a_{m,1} & \dots & a_{m,n} \end{pmatrix}, \tag{5}$$

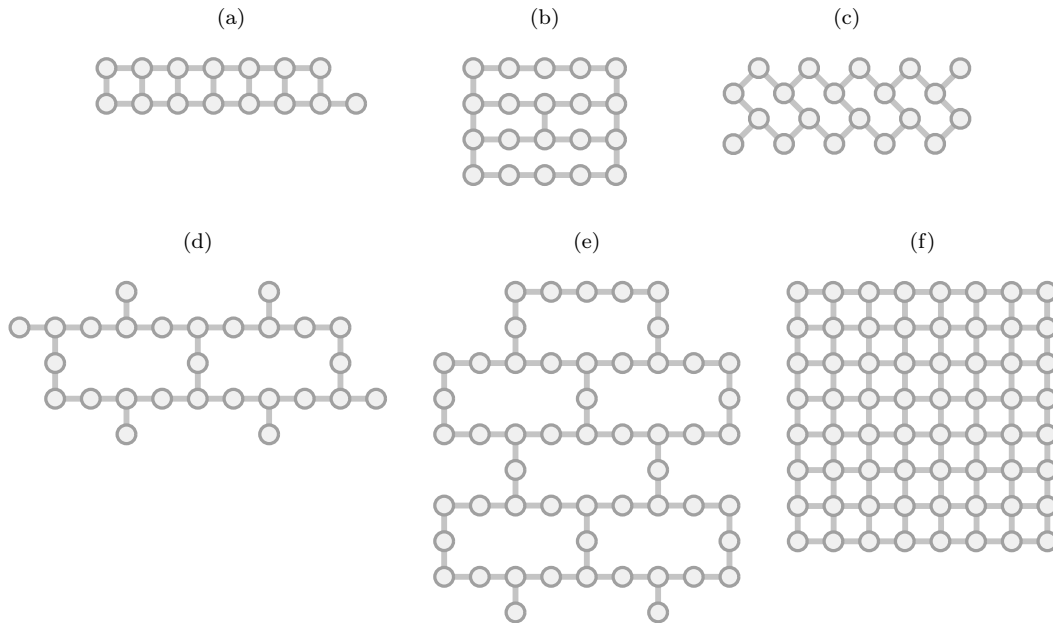


FIG. 1. The hardware graphs that were used as inputs to benchmark the multi-qubit pathfinding algorithm. **(a)** The 15-qubit *ibmq_16_melbourne* device [26]. **(b)** The 20-qubit *ibmq_poughkeepsie* device. **(c)** The 20-qubit Rigetti *Acorn* device [27]. In the actual device, one of the qubits is offline, resulting in 19 working qubits. **(d)** The 27-qubit *ibmq_paris* device. **(e)** The 53-qubit *ibmq_rochester* device. **(f)** A 64-qubit 8x8 Grid.

where each element $a_{i,j} \in \mathbb{R}$ specifies the impact of variable x_j on the i -th constraint.

This formulation allows LP to be a powerful tool, as it provides a structured way to optimise complex systems under constraints, ensuring that all specified conditions are met while achieving the best possible outcome with respect to the objective function.

B. Binary Integer Linear Programming (BILP)

In many real-world applications, the variables we aim to optimise over are not continuous but must be restricted to binary or integer values. This occurs when optimising with respect to discrete quantities, such as the number of cars produced, or decisions that involve logical relations, like whether to proceed with Project A if it precludes Projects B and C. For such cases, extended forms of mathematical programming come into play such as pure integer, binary integer, and mixed integer linear programming. Pure integer linear programs constrain all variables to integer values, binary integer linear programs (BILPs) restrict them to binary values, and mixed integer linear programs include both integer and real variables. Generally, linear programming problems that include variables that are limited to integer values (including binary) belong to the NP-hard complexity class [28]. This work focuses on BILP, which can be applied to a wide range of problems including the best choice problem (or secretary problem) [29], the travelling salesman problem, satisfiability problems, generalised assignment problems, and minimum weight cut problems [30, 31].

The standard form for a BILP can be written as

$$\max \mathbf{c} \cdot \mathbf{x}, \tag{6}$$

$$\text{such that } A\mathbf{x} \leq \mathbf{b}, \tag{7}$$

$$\text{where } x_i \in \{0, 1\}, \quad i = 0, 1, \dots, n, \tag{8}$$

where $\mathbf{c} = (c_1, c_2, \dots, c_n) \in \mathbb{R}^n$ are the coefficients of the objective function, $\mathbf{x} = (x_1, x_2, \dots, x_n) \in \{0, 1\}^n$ denotes the binary variables under consideration, and $\mathbf{b} = (b_1, b_2, \dots, b_m) \in \mathbb{R}^m$ is the vector of constants defining the upper

bounds in the constraints. The constraint matrix A is given by:

$$A = \begin{pmatrix} a_{1,1} & \dots & a_{1,n} \\ \vdots & \ddots & \vdots \\ a_{m,1} & \dots & a_{m,n} \end{pmatrix}, \quad (9)$$

where each element $a_{i,j} \in \mathbb{R}$ specifies the impact of variable x_j on the i -th constraint. While finding exact solutions to BILP problems is NP-hard, there exist efficient algorithms capable of approximating solutions with reasonable computational effort and accuracy [32–34].

C. Multi-Agent Pathfinding (MAPF)

Multi-agent pathfinding (MAPF) is relevant to various disciplines and optimisation problems. While single-agent scenarios can utilise fast and efficient algorithms such as the A^* pathfinding algorithm [35] or the Dijkstra’s pathfinding algorithm, the introduction of multiple agents introduces complexities due to the need for cooperation to avoid collisions and minimise interference with each other’s trajectories to achieve a globally optimal solution. Here, we focus on a problem referred to as time-dependent discrete routing on a collision-free unit-distance graph. It is characterised by discrete time steps where agents can complete any of their actions in exactly one time step, only one agent can occupy a single node at any time step, and agents cannot pass through each other.

Following the work in [36], the MAPF problem can be split into two primary variants: anonymous and non-anonymous pathfinding. Ideas from these two extremes can be generalised to form the combined target-assignment and pathfinding (TAPF) problem.

1. Anonymous Multi-Agent Pathfinding

In the anonymous variant of MAPF, agents are indistinguishable from one another and are collectively assigned to a set of destinations without specific assignments per agent. Consider a connected undirected graph $G(V, E)$ with nodes V representing possible locations and edges E representing possible movements, and each node includes a loop to allow agents to remain idle. Given N agents \mathbf{A} , with N source nodes \mathbf{S} and N destination nodes \mathbf{D} , the objective is to find optimal paths $p_a : \mathbb{Z} \rightarrow V$ for each agent $a \in \mathbf{A}$ that satisfy a range of conditions. The paths must map time step indices $0, 1, \dots, T$ to nodes such that consecutive positions $p_a(t)$ and $p_a(t+1)$ are either adjacent in G or identical (implying the agent remains idle). Additionally, the paths can revisit nodes, thus forming *trails* in graph-theoretical terms. The paths for the anonymous multi-agent pathfinding problem must satisfy the following conditions:

- **Exclusivity of location:** No two agents can occupy the same location at the same time step.
 $\forall a, b \in \mathbf{A}$ where $a \neq b$, and $\forall t \in \{0, 1, \dots, T\}$, then $p_a(t) \neq p_b(t)$.
- **Non-intersecting paths:** Agents cannot pass through each other.
 $\forall a, b \in \mathbf{A}$ where $a \neq b$, and $\forall t \in \{0, 1, \dots, T\}$, then $(p_a(t), p_b(t)) \neq (p_b(t+1), p_a(t+1))$.
- **Starting conditions:** Each agent starts at its assigned source location.
 $\forall a \in \mathbf{A}$, $\exists s \in \mathbf{S}$, such that $p_a(0) = s$.
- **Ending conditions:** Each agent ends at a destination location.
 $\forall a \in \mathbf{A}$, $\exists d \in \mathbf{D}$, such that $p_a(T) = d$.

The goal is to find valid paths p_a for each agent a that minimises the makespan T (number of time steps). This form of pathfinding can be solved using discrete dynamic network flow techniques [37], transforming the input graph G into a time-expanded graph as shown in Figure 2. Time steps are layered left to right in order of increasing time. Each time step consists of two copies of nodes V of G along with two additional nodes for each possible agent movement, as specified by edges in G . The edges in the time-expanded graph are determined from the transformation shown in Figure 2b. These edges facilitate rules preventing agents from moving through each other and ensure that only one agent occupies a location at any given time step, while permitting agents to either remain idle or move to an adjacent node. This problem can be modelled as a max flow or min-cost flow problem on the time-expanded graph by specifying source nodes in the initial layer $t = 0$ for starting locations and sink nodes in the final layer $t = T$ for end locations, with the edge capacities set to 1 to restrict each edge in the time-expanded graph to a single agent, and adding traversal costs as edge weights if using min-cost flow to minimise total traversal costs. The corresponding max flow

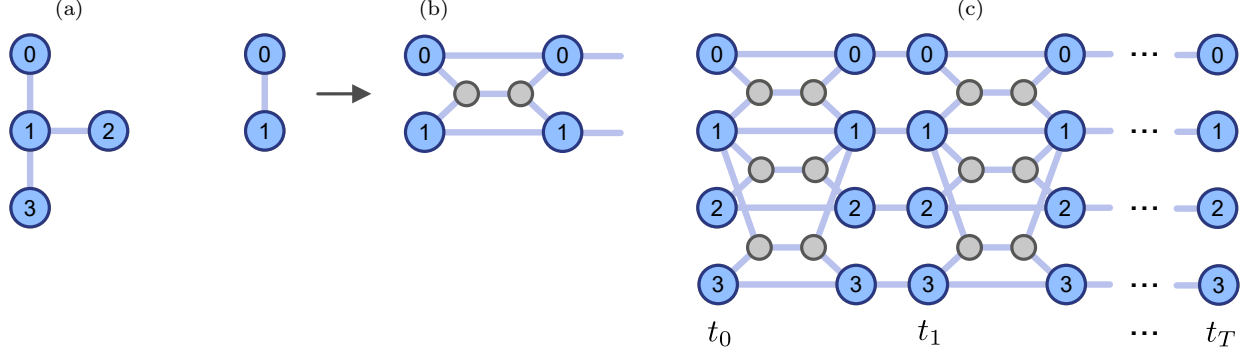


FIG. 2. An example of the anonymous multi-agent pathfinding time expansion graph transformation. **(a)** An undirected simple input graph G describing the possible agent locations and movements for a particular problem instance. **(b)** To expand the graph through time, an edge in the original graph can be transformed as shown. This transformation enables agents to either be idle or move to an adjacent node for the next time step. The additional two grey nodes enforce the rule that only one agent can use the movement edge per time step, this is required to stop the agents moving through each other. The outgoing edges to the very right are used to enforce that only one agent can be at any one location per time step. **(c)** The input graph is converted to a time-expanded graph with T time steps labelled t_0, t_1, \dots, t_T . Two copies of the original input graph nodes are used for each time step layer, along with an additional two nodes for each edge.

or min-cost flow algorithms, such as the fast and efficient Edmonds-Karp algorithm [38], are performed incrementally on increasing values of maximum time step T , starting at $T = 0$, until a valid solution is found, indicating the optimal makespan. It has been shown that there will always be a feasible solution (as long as the graph G is connected) and that the optimal makespan is always no larger than $N + |V| - 1$, where $|V|$ is the number of nodes [37].

2. Non-Anonymous Multi-Agent Pathfinding

In the non-anonymous variant of MAPF, each agent is uniquely identified and assigned to a specific target destination, which is not shared with any other agent. This problem is prevalent in fields such as video games, robotics, and automated warehouse systems [39–42]. The problem is NP-hard and the optimal makespan solution is bounded by $\mathcal{O}(|V|^3)$. There are a variety of existing strategies for solving this problem, including ILP [43], satisfiability [44], answer set programming [45], and search based methods [46–50].

3. Combined Target-Assignment and Pathfinding (TAPF)

The ideas of anonymous and non-anonymous MAPF can be generalised with each representing extreme cases of the broader problem. The TAPF problem involves assigning target destinations to agents and subsequently finding collision-free paths to these destinations, all while minimising the makespan. There are multiple teams of agents, where each team is allocated a set of destinations that can be shared internally but not with agents from other teams. As a generalisation of non-anonymous MAPF, TAPF is also NP-hard (even for two teams) and the optimal makespan solution remains bounded by $\mathcal{O}(|V|^3)$. There are various existing approaches to solve TAPF, including conflict-based min-cost flow (CBM) [36], multi-commodity flow [36, 43], and answer set programming [51].

The CBM approach is a particularly popular approach to TAPF. It is a hierarchical algorithm with distinct high and low levels of processing. At the higher level it considers each team as a single meta-agent and uses conflict-based search (CBS) [49, 52] to resolve collisions between each team. CBS uses a breadth-first search on a tree where each node in the tree contains paths for each team alongside a set of constraints. When collisions occur, the tree is expanded with nodes that apply direct constraints to avoid the conflict—for example, if team 1 and 2 have a collision at an edge, two nodes are added: one restricts team 1 from using the edge, and the other restricts team 2. For each node, new paths are recalculated for the teams with their additional constraints. At the lower level, paths for each team are determined using an anonymous multi-agent pathfinding algorithm, which can be performed in polynomial time.

Another approach, of which is particularly interesting to the application of qubits, is the multi-commodity flow method, which addresses scenarios of max flow or min-cost flow where there is more than one commodity. Each commodity has its own flow demand with different source and destination nodes, and the flow capacity of network

edges is shared among all commodities. In the following sections, we demonstrate how multi-commodity flow can be adapted into a BILP to effectively model the *multi-qubit pathfinding problem*.

D. The Token Swapping Problem (TSP)

In physical quantum devices, the movement of logical qubits—each encoded as the state of a single physical qubit—is primarily actioned using SWAP gates. Consequently, in the context of quantum computing, pathfinding typically involves swap-based movement of logical qubits. The makespan of the resulting solution directly corresponds to the SWAP depth of the mapped circuit. Within the computer science community, this problem is a variant of the more generally known token swapping problem (TSP).

The TSP, as defined in the literature [53, 54], involves placing a token on each node of a connected simple graph G . The objective is to manoeuvre these tokens from their initial positions to assigned destinations via swap operations, minimising the total number of swaps. Only one pair of tokens can be swapped at a time. The TSP is generally NP-hard [55–57] but has been solved in polynomial time on specific graph structures such as paths, cycles, complete graphs, and complete bipartite graphs [54, 58, 59].

There are many variants to the TSP. A notable variant is the *c-coloured token swapping problem* (*c*-CTSP) [54], where tokens and nodes are assigned one of c possible colours. The goal here is to manoeuvre the tokens such that each node has a token of its assigned colour, essentially routing coloured tokens to achieve a permutation to the final node-colour configuration starting from the initial token-colour configuration. The 2-CTSP has been shown to be solvable in polynomial time, whereas the 3-CTSP is NP-complete [54]. Another variant is the *parallel token swapping problem* (PTSP) [55], which permits any number of disjoint pairs of tokens to be simultaneously swapped in the same time step, unlike the TSP that only allows a single swap operation at a time. Like the TSP, the PTSP has been shown to be NP-complete. These two variants can be combined to form the *parallel c-coloured token swapping problem* (*c*-PCTSP), which is NP-hard, even when limited to 2-PCTSP with only two colours.

III. MULTI-QUBIT PATHFINDING (MQPF)

In this section, we detail the MQPF problem and introduce our MQPF algorithm that solves it. In quantum compilation literature, the MQPF problem usually refers to certain variations of the token swapping problem (TSP). The primary MQPF problem addressed in our work for K teams of qubits can be summarised as the weighted variant of the parallel $(K + 1)$ -coloured token swapping problem ($(K + 1)$ -PCTSP), discussed in the previous section. The extra colour represents physical qubit locations not occupied by logical qubit states. This problem is NP-hard, even for a single team.

Numerous algorithms exist for approaching variations of the MQPF problem. These include algorithms based on propositional satisfiability (SAT) [22, 23], Pseudo-Boolean Optimisation [24], recursive subcircuit cutting [1], and ILP (independently developed to our work, using a different modelling approach) [5]. These techniques typically aim to minimise either the SWAP gate count or the SWAP depth—total number of time steps—in the mapped circuit, and with each logical qubit operating as its own independent team.

Given the prevalence of noise introduced through qubit decoherence and the application of two-qubit gates on physical quantum devices, it is important to minimise the computation time and the total gate error introduced. To do this, our model focuses on minimising the SWAP depth primarily, followed by minimising the accumulated SWAP gate error as a secondary objective. In addition to solving this problem, our algorithm supports flexibility in the assignment of logical qubit teams and destination nodes. Teams of qubits can share destinations, and the number of destinations for each team can exceed the number of qubits in the team. The teams can then be routed to any subset of their assigned destinations.

We formally define the MQPF problem as follows:

Definition 1 (The MQPF Problem). Consider a connected hardware graph $G(V, E)$, where nodes V correspond to qubits and edges E correspond to possible applications of two-qubit gates (such as CNOTs and SWAPs). Given N logical qubits, partitioned into K disjoint teams $\mathbf{A} = \mathbf{A}_1 \cup \mathbf{A}_2 \cup \dots \mathbf{A}_K$, with each team assigned disjoint sets of source and destination locations $\mathbf{S} = \mathbf{S}_1 \cup \mathbf{S}_2 \cup \dots \mathbf{S}_K$ and $\mathbf{D} = \mathbf{D}_1 \cup \mathbf{D}_2 \cup \dots \mathbf{D}_K$, where $|\mathbf{A}_k| = |\mathbf{S}_k| = |\mathbf{D}_k|$ (although the model allows for $|\mathbf{A}_k| \leq |\mathbf{D}_k|$ and overlapping destination partitions \mathbf{D}_k). For each logical qubit $a \in \mathbf{A}$, find a path through time $p_a : \mathbb{Z} \rightarrow V$ which maps time step indices $0, 1, \dots T$ to nodes in G such that for all time steps t , either $p_a(t)$ and $p_a(t + 1)$ are adjacent in G or $p_a(t) = p_a(t + 1)$. Each path must satisfy the following conditions:

- **Exclusivity of location:** No two logical qubits can occupy the same location at the same time step.
 $\forall a, b \in \mathbf{A}$ such that $a \neq b$, and $\forall t \in \{0, 1, \dots T\}$, then $p_a(t) \neq p_b(t)$.

- **Swap-based movement:** Logical qubits must swap when moving to an occupied location.
 $\forall a \in \mathbf{A}$ and $\forall t \in \{0, 1, \dots, T\}$, if $\exists b \in \mathbf{A}$ such that $p_a(t+1) = p_b(t)$, then $p_b(t+1) = p_a(t)$.
- **Starting conditions:** All logical qubits must start at sources corresponding to their team.
 $\forall a_k \in \mathbf{A}_k, \exists s_k \in \mathbf{S}_k$, such that $p_{a_k}(0) = s_k$.
- **Ending conditions:** All logical qubits must end at destinations corresponding to their team.
 $\forall a_k \in \mathbf{A}_k, \exists d_k \in \mathbf{D}_k$, such that $p_{a_k}(T) = d_k$.

The primary objective of the problem is to find valid paths through time p_a for each logical qubit a that minimises the SWAP depth, T (number of time steps). For the secondary objective, gate error rates are assigned to each possible SWAP operation in the hardware graph, aiming to minimise the combined total error rate of logical qubit paths, \mathcal{E} . Since quantum gate errors are multiplicative, the accumulated error rate of the SWAP gate schedule is calculated as

$$\mathcal{E} := 1 - \prod_{\alpha \in \{\text{SWAPs}\}} (1 - \epsilon_\alpha)^3, \quad (10)$$

where ϵ_α is the error rate of the CNOT used to perform SWAP gate α , and $(1 - \epsilon_\alpha)^3$ is the success rate of the SWAP gate (since three CNOTs are used for each SWAP).

A. The MQPF Algorithm

The general strategy of our algorithm is highlighted in Figure 3. We begin by time expanding the input hardware graph as shown in Figure 3b, similar to the approach used for anonymous multi-agent pathfinding discussed in Section II C. In this expansion, each vertical layer, progressing from left to right, duplicates the hardware graph nodes and represents a single time step—defined as the duration required to execute a SWAP gate. These layers are labelled t_0, t_1, \dots, t_T . Each edge in the expansion represents possible movements that a logical qubit can undertake when progressing through time steps; this includes remaining idle or swapping locations with adjacent physical qubits in the hardware graph.

The time expansion process for MQPF is more straightforward than for MAPF because we model it using binary integer linear programming (BILP). This approach allows the constraints to be programmed directly into the model rather than using gadgets in the expanded graph. Once the hardware graph has been time expanded, we define teams of source and destination locations at the initial and final layers of the expanded graph, respectively. To accomplish this, special source $\mathbf{I} = \{I_1, I_2, \dots, I_K\}$ and destination $\mathbf{F} = \{F_1, F_2, \dots, F_K\}$ nodes, representing teams, are attached to the initial and final layers. These nodes are linked to their respective team source and destination locations, as demonstrated in Figure 3c.

To determine the optimal paths for logical qubits through time, corresponding to the minimal SWAP depth, the algorithm initially expands to a depth $T = 0$ and uses a BILP solver to search for a solution. If no solution is found, the graph is expanded to $T = 1$, and the process is repeated. This iterative expansion and solution search continues until a solution is discovered, at which point the depth T is confirmed as the optimal SWAP depth. It has been shown that a solution will always exist and the number of time steps is bounded by $\mathcal{O}(|V|^2)$, where $|V|$ is the number of nodes in the graph G [60].

When solving the BILP at each time step, the accumulated gate error $\mathcal{E} = 1 - \prod_{\alpha \in \{\text{SWAPs}\}} (1 - \epsilon_\alpha)^3$ can be optimised using the linear objective function by equivalently minimising $C := -\log(1 - \mathcal{E})$ as the total cost. Substituting the expression for the accumulated gate error \mathcal{E} gives the following objective value

$$C = - \sum_{\alpha \in \{\text{SWAPs}\}} 3 \log(1 - \epsilon_\alpha), \quad (11)$$

where $c_\alpha := -3 \log(1 - \epsilon_\alpha)$ are the corresponding costs for each SWAP gate α used in the solution. The objective value can be converted back to the accumulated error rate of the swap schedule using

$$\mathcal{E} = 1 - 1/\exp(C). \quad (12)$$

The MQPF algorithm can be adjusted to further optimise for the accumulated error by considering solutions with higher SWAP depths, which may involve a trade-off between the optimisation quality of the primary and secondary objectives.

We will describe how the BILP is constructed in the following sections.

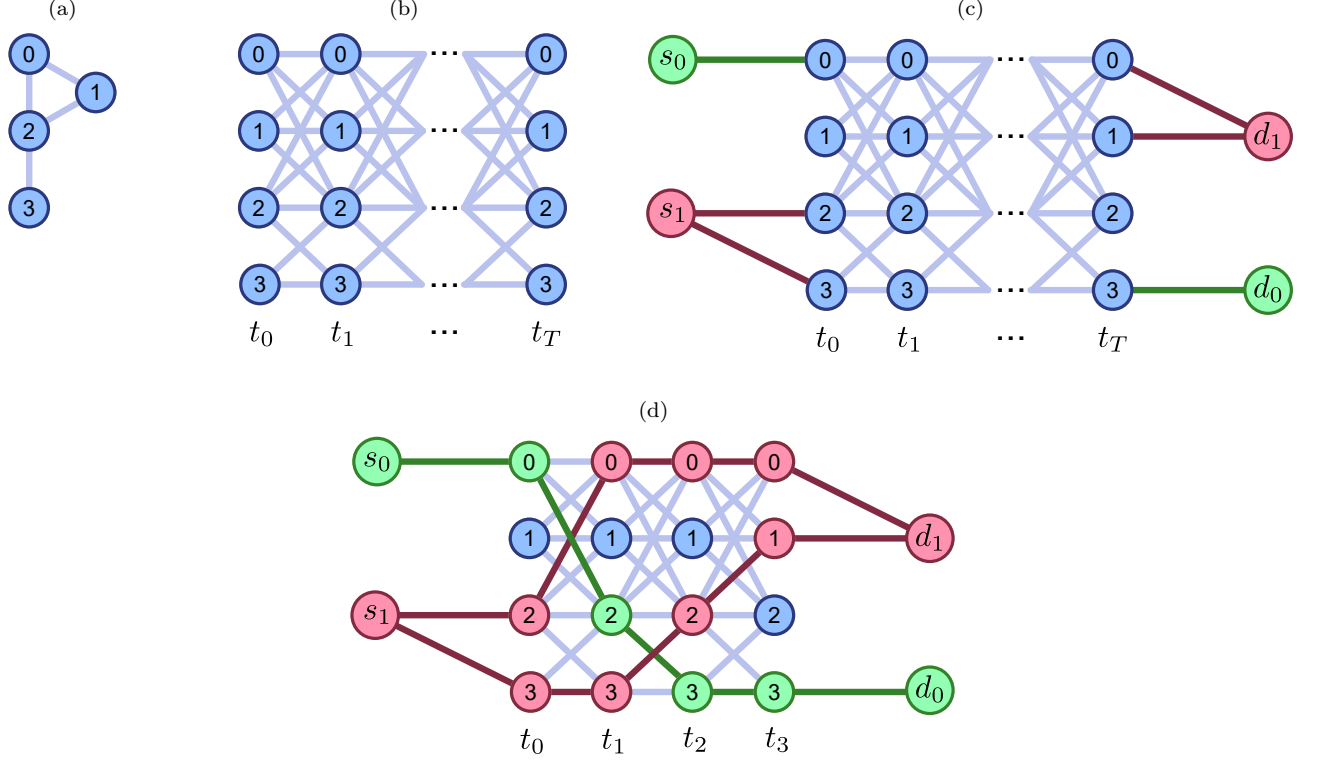


FIG. 3. An example of the process used when modelling a problem instance. **(a)** The initial hardware layout where nodes represent physical qubits and edges represent connected pairs of qubits that could be operated on by entanglement generating gates such as CNOTs. **(b)** The initial layout is converted to a time-expanded graph where layers represent time steps (where a time step is the amount of time required to perform a SWAP operation) labelled t_0, t_1, \dots, t_T and edges represent possible movements that logical qubits could take between them. The possible movements only include being idle and swapping locations between connected physical qubits in the hardware layout. **(c)** Source and destination locations can be specified in the time-expanded graph by attaching special nodes (s_0, s_1, d_0, d_1) to the initial and final layers respectively. In this example, there are two teams of logical qubits to be routed. Team 0 contains one logical qubit starting at q0 and ending at q3 while Team 1 contains two logical qubits starting at q2 and q3, and ending at q0 and q1. **(d)** The solution to this example problem instance with a SWAP depth of three (since the route has a total of three time steps).

1. Multi-Commodity Flow Problem

Our approach to finding valid paths on a time-expanded graph draws inspiration from the multi-commodity flow problem. We will begin by constructing the linear program for multi-commodity flow on the time-expanded graph as a base, then modify it to obtain the BILP for the MQPF problem. The multi-commodity flow problem typically represents scenarios in network flow where multiple flows, each corresponding to a distinct commodity, need routing through a network. A classical example is the telecommunication routing problem, where messages are routed through a network to minimise costs associated with transmission line variables such as packet delay and bandwidth utilisation [61]. In such models, network nodes represent traffic origin and destination stations and edges represent transmission lines. The objective is to route a specified amount of messages from the origins to the destinations without exceeding the capacity of any transmission line, all while minimising the total cost.

For the quantum hardware layout, we adopt a similar approach but apply it to a time-expanded graph. This adaptation can be modelled through the following linear program.

Objective Function:

$$\min \sum_{k \in \{1, \dots, K\}} \sum_{t \in \{1, \dots, T\}} \sum_{(i,j) \in E} c_{ij} x_{ij,t}^k, \quad (13)$$

where $\{1, \dots, K\}$ are the commodities (teams of qubits), $\{1, \dots, T\}$ are the time steps, $(i,j) \in E$ are the edges in the hardware graph G connecting nodes i and j from the set of nodes V of G , c_{ij} is the cost weight of edge (i,j) , and

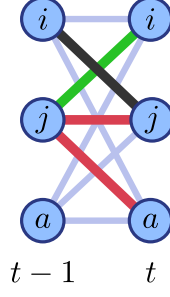


FIG. 4. A graphic representing Constraint (6) introduced in Adjustment 4 of Section III A 2 which enforces swap-based movement when adapting the linear program from multi-commodity flow to multi-qubit pathfinding. If the logical qubit at location i time step $t-1$ moves to location j time step t (shown in black), then the logical qubit at location j time step $t-1$, in this example, cannot move to locations j nor a at time step t (shown in red). Therefore, the only movement possible for logical qubit at location j time step $t-1$ is to location i time step t (shown in green).

$x_{ij,t}^k$ is the flow of commodity k through edge (i,j) from i at time $t-1$ to j at time t .

Constraints:

- (1) **Conservation of flow:** $\forall k \in \{1, \dots, K\}, \forall t \in \{1, \dots, T-1\}, \forall i \in V, \sum_{j \in V} x_{ji,t}^k - \sum_{j \in V} x_{ij,t+1}^k = 0,$
 $\forall k \in \{1, \dots, K\}, \forall i \in \mathbf{S}_k, x_{I_k i} - \sum_{j \in V} x_{ij,1}^k = 0,$
 $\forall k \in \{1, \dots, K\}, \forall i \in \mathbf{D}_k, \sum_{j \in V} x_{ji,t_{T-1}}^k - x_{i F_k} = 0,$
- (2) **Edge flow capacity:**
 $\forall t \in \{1, \dots, T\}, \forall (i,j) \in E, \sum_{k \in K} x_{ij,t}^k \leq u_{ij},$
- (3) **Maximum flow for source and destination edges:**
 $\forall k \in \{1, \dots, K\}, \forall i \in \mathbf{S}_k, x_{I_k i} = u_{I_k i},$
 $\forall k \in \{1, \dots, K\}, \forall i \in \mathbf{D}_k, x_{i F_k} = u_{i F_k},$
- (4) **Real variables:**
 $\forall k \in \{1, \dots, K\}, \forall t \in \{1, \dots, T\}, \forall (i,j) \in E, x_{ij,t}^k \in \mathbb{R},$

where the variables $x_{I_k i}$ and capacities $u_{I_k i}$ correspond to flows and max flows from the attached special source node I_k to source nodes $i \in \mathbf{S}_k$ and the variables $x_{i F_k}$ and capacities $u_{i F_k}$ correspond to flows and max flows from destination nodes $i \in \mathbf{D}_k$ to the attached special destination node F_k . The capacities u_{ij} represent the maximum allowable flow through edge $(i,j) \in E$ of G at any time step.

2. Adapting Multi-Commodity Flow to MQPF

The multi-commodity flow linear program can be modified to mimic the behaviour of teams of logical qubits traversing a hardware graph via SWAP gates. The following four adjustments can be made to achieve this:

1. **Modification of Variables to Binary:** The variables are changed to binary, modifying Constraint (4) as:

- (4) Binary variables:
 $\forall k \in \{1, \dots, K\}, \forall t \in \{1, \dots, T\}, \forall (i,j) \in E, x_{ij,t}^k \in \{0, 1\}.$

With this adjustment, each variable $x_{ij,t}^k$ now decides whether a logical qubit from team k is traversing the edge in the time-expanded graph or not.

2. **Setting Flow Capacities to One:** To enforce that no more than one logical qubit traverses any edge in the time-expanded graph at a time, all flow capacities are set to one:

- $\forall (i,j) \in E, u_{ij} = 1,$
- $\forall k \in \{1, \dots, K\}, \forall j \in \mathbf{S}_k, u_{I_k j} = 1,$
- $\forall k \in \{1, \dots, K\}, \forall i \in \mathbf{D}_k, u_{i F_k} = 1.$

3. Enforcing Exclusivity of Location: A fifth constraint is introduced to limit each location in the time-expanded graph to a maximum of one logical qubit per time step:

(5) Exclusivity of location:

$$\forall t \in \{1, \dots, T\}, \quad \forall i \in V, \quad \sum_{k=1}^K \sum_{j \in V} x_{ji,t}^k \leq 1.$$

4. Enforcing Swap-Based Movement: A sixth constraint is introduced to enforce the swapping behaviour of logical qubits:

(6) Swap-based movement:

$$\forall t \in \{1, \dots, T\}, \quad \forall (i, j) \in E, \quad \sum_{k=1}^K x_{ij,t}^k + \sum_{k=1}^K \sum_{l \in V, \text{s.t. } l \neq i} x_{jl,t}^k \leq 1.$$

To help better understand Adjustment 4, a graphical representation of the newly added Constraint (6) is shown in Figure 4. The constraint ensures that if a logical qubit traverses from location i to j at time step t , then any qubit at j in the previous time step can only move to location i . To see how this works in more detail, we can look at each term separately. The first summation term in the inequality is over the flows along edge (i, j) which maximises at 1 due to the total number of logical qubits that can travel through an edge being limited by a capacity of 1. The second summation term is over all flows from location j that do not go to location i in time step t . The sum is always a maximum of 1 since all variables $x_{jl,t}^k$ in the sum correspond to possible movement options for a logical qubit at location j and there can only be one logical qubit at any location at any time (as per Constraint (5)). Adding the two summation terms together and requiring them to be no more than 1 forces a maximum of only one term to be equal to 1. Thus, both of the following cannot be simultaneously true in the same time step: that logical qubit at i moves to j and logical qubit at j moves to somewhere that is not i , hence enforcing the swap behaviour.

3. The final BILP for the MQPF problem

The BILP used to search for a solution at each time step during the iterative time expansion of our MQPF algorithm can be summarised as follows.

Objective Function:

$$\min \sum_{k \in \{1, \dots, K\}} \sum_{t \in \{1, \dots, T\}} \sum_{(i,j) \in E} c_{ij} x_{ij,t}^k, \quad (14)$$

where $\{1, \dots, K\}$ are the teams of qubits, $\{1, \dots, T\}$ are the time steps, $(i, j) \in E$ are the qubit-pair edges in the hardware graph G , $c_{ij} := -3 \log(1 - \epsilon_{ij})$ is the cost for a SWAP gate to be applied to qubit pair (i, j) (specified in Equation 11), and $x_{ij,t}^k$ specifies whether a team k qubit traverses qubit-pair (i, j) from qubit i at time $t-1$ to qubit j at time t .

Constraints:

(1) **Conservation of flow:**

$$\begin{aligned} \forall k \in \{1, \dots, K\}, \quad \forall t \in \{1, \dots, T-1\}, \quad \forall i \in V, \quad \sum_{j \in V} x_{ji,t}^k - \sum_{j \in V} x_{ij,t+1}^k &= 0, \\ \forall k \in \{1, \dots, K\}, \quad \forall i \in \mathbf{S}_k, \quad x_{I_k i} - \sum_{j \in V} x_{ij,1}^k &= 0, \\ \forall k \in \{1, \dots, K\}, \quad \forall i \in \mathbf{D}_k, \quad \sum_{j \in V} x_{ji,t_{T-1}}^k - x_{i F_k} &= 0, \end{aligned}$$

(2) **Edge flow capacity:**

$$\forall t \in \{1, \dots, T\}, \quad \forall (i, j) \in E, \quad \sum_{k \in K} x_{ij,t}^k \leq 1,$$

(3) **Maximum flow for source and destination edges:**

$$\begin{aligned} \forall k \in \{1, \dots, K\}, \quad \forall i \in \mathbf{S}_k, \quad x_{I_k i} &= 1, \\ \forall k \in \{1, \dots, K\}, \quad \forall i \in \mathbf{D}_k, \quad x_{i F_k} &= 1, \end{aligned}$$

(4) **Binary variables:**

$$\forall k \in \{1, \dots, K\}, \quad \forall t \in \{1, \dots, T\}, \quad \forall (i, j) \in E, \quad x_{ij,t}^k \in \{0, 1\},$$

(5) **Exclusivity of location:**

$$\forall t \in \{1, \dots, T\}, \quad \forall i \in V, \quad \sum_{k=1}^K \sum_{j \in V} x_{ji,t}^k \leq 1,$$

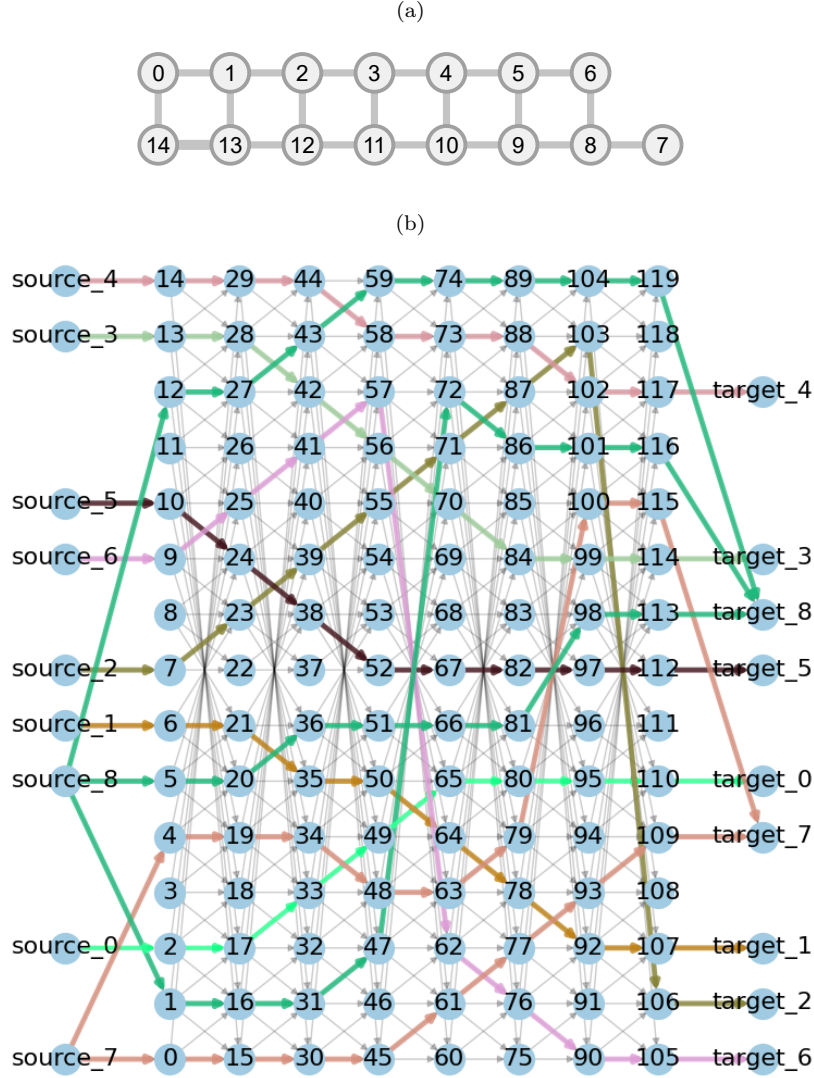


FIG. 5. An example multi-qubit pathfinding solution for a random problem instance on the 15-qubit *ibmq_16_melbourne* device. (a) The *ibmq_16_melbourne* device qubit layout. (b) Each attached special source node, labelled ‘source_’ i , is assigned a colour corresponding to a team i of logical qubits and directed edges connect to corresponding source nodes. The attached special destination nodes for team i are labelled ‘target_’ i and have edges connecting to the corresponding destination nodes. The coloured paths of edges correspond to paths through time for each logical qubit in the optimal SWAP-depth solution to the example multi-qubit pathfinding problem instance.

(6) **Swap-based movement:**

$$\forall t \in \{1, \dots, T\}, \forall (i, j) \in E, \sum_{k=1}^K x_{ij,t}^k + \sum_{k=1}^K \sum_{l \in V, \text{s.t. } l \neq i} x_{jl,t}^k \leq 1.$$

The program can be further tailored to accommodate scenarios where destination nodes outnumber source nodes, and where multiple teams may share some destination nodes. Such flexibility is beneficial when the precise assignment of destination nodes is part of the optimisation problem, allowing for some leeway in these assignments. This can be implemented by removing the requirement for maximum flow at all destination edges (previously specified in Constraint (3)). By maintaining flow conservation, along with maximum flow constraints at all source edges, the program ensures that each logical qubit navigates through the time-expanded graph to the correct special destination node F_k associated with its team. In addition to enhancing the program’s flexibility, it can also reduce the optimal SWAP depth and hence computation time by broadening the range of destination options available for logical qubits.

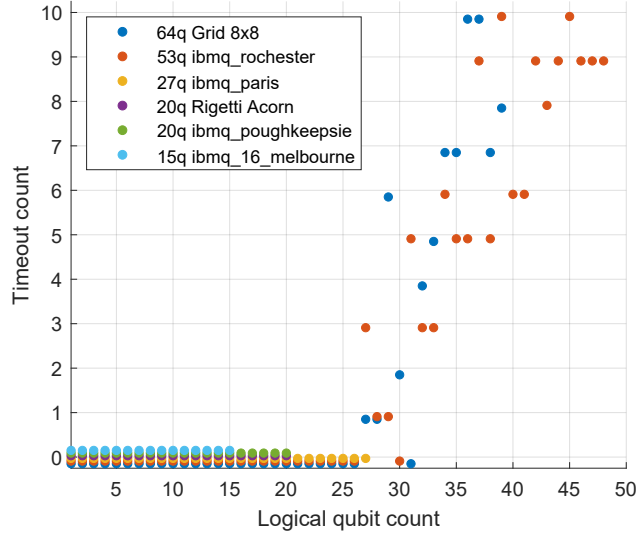


FIG. 6. The number of timeouts that occurred when multi-qubit pathfinding numbers of independent logical qubits (in their own teams) on the physical device layouts shown in Figure 1. Each data point is the number of random instances out of 10 that exceed 1000 seconds of computation time. Note that all instances that were above 39 independent logical qubits on the 64-qubit 8x8 grid timed out. All instances that time out are abandoned and ignored in the results. There is a small offset along the vertical axis of each device for the purpose of displaying overlapping data points.

IV. RESULTS

A. MQPF on Physical Qubit Layouts

The multi-qubit pathfinding (MQPF) algorithm described above was programmed in Python. The script inputs a hardware graph, logical qubit teams, and their corresponding source and destination locations. It then automatically time expands the hardware graph incrementally for increasing depth and generates the corresponding binary integer linear programs (BILPs). Each program is solved using Gurobi commercial optimiser which specialises in solving mathematical programs [62]. Computations were performed on an Intel Core i5-6500 CPU 3.2 GHz running Windows 10 with 16GB RAM. Instances exceeding 1000 seconds of computation time were recorded and abandoned. When a solution is found, it can be used to construct the paths through time for each of the logical qubits. An example of a solution for a random problem instance on the *ibmq_16_melbourne* device is shown in Figure 5.

In our implementation, we improve the algorithm’s computational efficiency using the following two optimisations:

1. Trim impossible variables.
2. Presolve using faster algorithms to obtain SWAP-depth lower bounds.

In Optimisation 1, all variables corresponding to edges that are impossible to reach for the associated variable’s team are removed. This is done with a sweep forwards in time to remove variables for edges that logical qubits cannot reach and then a sweep backwards in time to remove variables for edges that logical qubits cannot use, because if they did, they would not be able to reach any of their destination nodes by the final time step. In Optimisation 2, each iteration of the time expansion is first solved using a fast algorithm with a solution that is a lower-bound of the SWAP-depth solution. The same MQPF algorithm can be used to achieve this when all logical qubits are assigned to the same team, since the computation speed can become orders of magnitude faster. Another fast lower-bound algorithm approach is to use Dijkstra’s pathfinding algorithm to obtain the maximum length over teams, where each team length is calculated as the minimum path distance over individual paths from source nodes to target nodes in the same team. Then, once a solution is found, the time expansion procedure continues but with the qubits assigned to their usual teams and the depth starting at the depth of the found solution. We do this because the computation time for finding a solution with all qubits on the same team is significantly lower than on multiple teams. Optimality is not lost since the optimal SWAP-depth for multiple teams is always greater than or equal to that of a single team for the same source and destination locations on the hardware graph.

We benchmark various aspects of the algorithm applied to a variety of hardware graphs shown in Figure 1 by solving random problem instances. In all of the following computations, instances that exceeded 1000 seconds with respect to

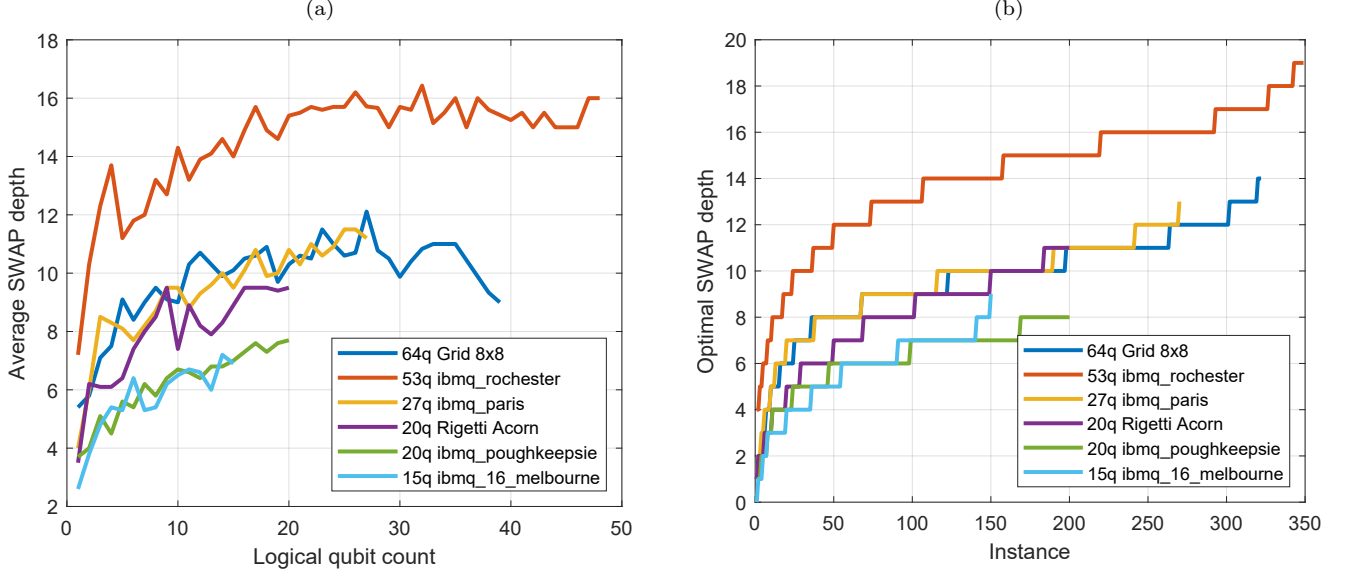


FIG. 7. Solution SWAP depths for multi-qubit pathfinding logical qubits implemented on physical device layouts shown in Figure 1. There are 10 random instances for each number of logical qubits, starting at one and ending at the number of physical qubits in the corresponding hardware graph. Each logical qubit is in its own team. Problem instances that exceed 1000 seconds are considered timed out and are ignored, with the number of instances timed out for each number of logical qubits shown in Figure 6. **(a)** The average optimal SWAP depths for each number of logical qubits. The SWAP depths appear to plateau as the number of logical qubits increases, which could be due to the instances with higher SWAP depths being more likely to timeout. **(b)** Optimal SWAP depths for all instances sorted in ascending order.

the single CPU machine were ignored in the results, the total number of timeouts that occurred for each problem size is shown in Figure 6. First we focus on the cases where each logical qubit is in its own team and measure the optimal SWAP depths as shown in Figure 7. The first plot shows the average solution SWAP depth over 10 random instances for increasing numbers of logical qubits (starting at one and ending at the number of qubits in the corresponding hardware graph), while the second plot shows solution SWAP depths for all of the random instances sorted in order of increasing optimal SWAP depth. When comparing the 53-qubit Rochester device and 64-qubit 8x8 grid, there is a considerable reduction in solution SWAP depth for the grid, even though it consists of more qubits. This is likely due to its connectivity, the average number of qubits each qubit is connected to is higher for the grid than for the Rochester device. This allows the logical qubits to find more direct paths to their destinations.

Next, we measure the optimised accumulated error rates for the time-expanded graphs at the optimal SWAP depths, shown in Figure 8. The average accumulated error over 10 random instances for each number of logical qubits is shown in Figure 8a. The accumulated error for all of the random instances sorted in order of increasing error rate is shown in Figure 8b. The CNOT errors (where 3 CNOT gates are used to implement a SWAP gate) assigned to physical qubit connections are randomly chosen using a log scale truncated normal distribution with a CNOT error mean of 0.001 and a \log_{10} variance of 0.5. A log scale normal distribution is used because it roughly matches the distributions of CNOT error rates found in the *ibmq_melbourne* and *ibmq_rochester* devices, although both with a \log_{10} standard deviation of approximately 0.165. The larger variance was chosen in the experiments to more clearly compare the differences between the devices. The 64-qubit 8x8 grid showed a considerable improvement over the other devices even though it has more physical qubits. This is likely due to the following two reasons. The first is that the 8x8 grid results in shallower optimal SWAP depths than some smaller devices such as the *ibmq_rochester* device, shown in Figs. 7a and 7b. Shallower SWAP depths typically use fewer SWAP gates, hence fewer sources of error. The second reason for the 8x8 grid's performance is that with the higher connectivity, there are more qubit neighbour options for each logical qubit to swap with, thus providing more opportunities to swap along connections with lower physical error rates.

The variance used for the distribution of CNOT-gate errors on the hardware graph can influence the accumulated error rates of optimised qubit paths. To investigate its impact, we measured the average optimal accumulated error for pathfinding random instances of 10 independent logical qubits on hardware graphs that are assigned random CNOT error rates sampled from distributions of increasing log variance. The results are shown in Figure 9. Each data point is the average of 100 random problem instances where each instance has newly randomised CNOT-errors

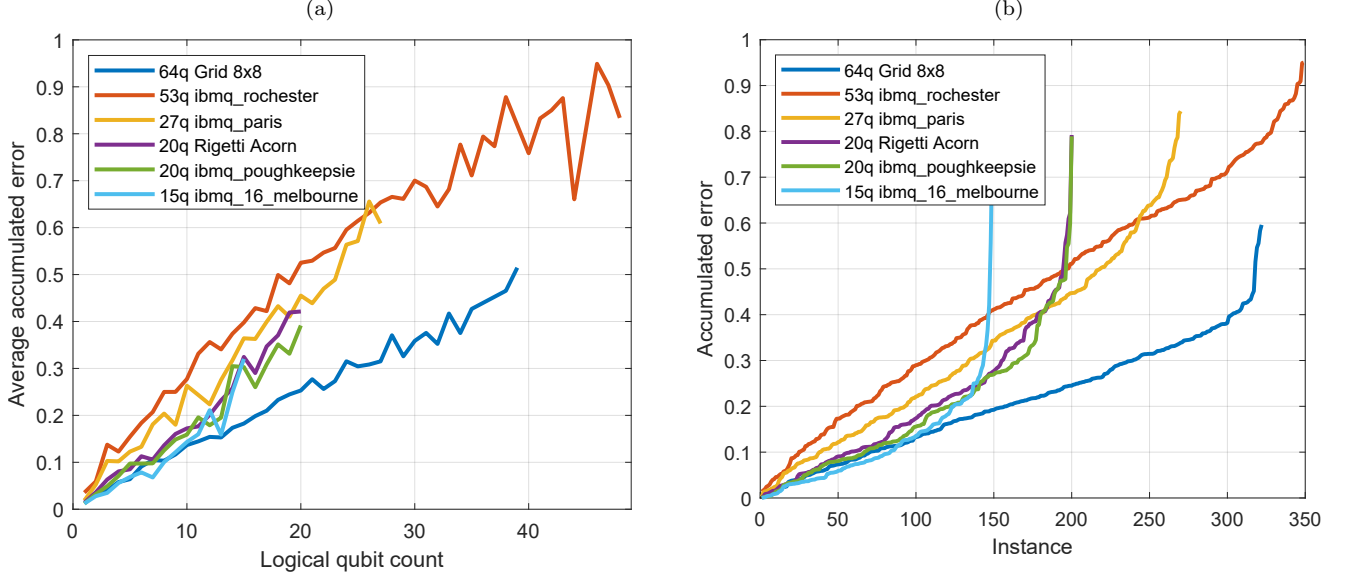


FIG. 8. Optimised accumulated error rates in solutions to multi-qubit pathfinding logical qubits on physical device layouts shown in Figure 1. There are 10 random instances for each number of logical qubits. The CNOT errors are randomised for each instance from a truncated normal distribution on a log scale with a mean of 0.001 and a \log_{10} error variance of 0.5. Each logical qubit is in its own team. Problem instances that exceed 1000 seconds are considered timed out and are ignored, with the number of instances timed out for each number of logical qubits shown in Figure 6. **(a)** The average accumulated error rates for each number of logical qubits. The variance of the accumulated errors increases due to there being more timeouts for higher numbers of logical qubits. **(b)** Accumulated error rates for all instances sorted in ascending order.

on the hardware graph. The results show that accumulated error rates tend to increase for increasing CNOT-error variance. This is likely due to the multiplicative nature of gate errors making high error gates far more impactful than low error gates. However, on the 64-qubit 8x8 grid, the accumulated error rates initially decrease until a CNOT \log_{10} error standard deviation of approximately 0.45, where it begins to increase. This initial decrease is likely due to the higher connectivity providing more opportunities to avoid higher error-rate CNOT gates, and a lower variance means that whatever higher error-rate gates that are included tend to be less extreme.

The average runtime over 10 random instances was measured for increasing numbers of logical qubits and the results are plotted in Figure 10a. The runtimes for all of the instances are plotted in Figure 10b, sorted in ascending order. The runtime generally increases for increasing numbers of variables and constraints in the BILP corresponding to the problem instance. Thus, solutions for larger hardware graphs typically take longer to compute. Although, hardware graphs with higher connectivity typically result in lower SWAP depth solutions, leading to shorter computation times. This can be seen, for example, when comparing results for the 64-qubit 8x8 grid against the 53-qubit *ibmq_rochester* device. The grid has comparable runtimes to the *ibmq_rochester* device even though it contains 20% more physical qubits and 93% more edges, adding variables and constraints to the BILP for the same time-expanded depth.

Finally, we investigate the effects of team sizes on computational runtimes. The runtimes for 10 random instances on the 64-qubit 8x8 grid hardware graph for increasing numbers of logical qubits are plotted in Figure 11. Three cases were compared: independent logical qubits that are each in their own team; logical qubits that are randomly assigned to a random number of teams; and a single team consisting of all logical qubits. The algorithm scales significantly better with fewer numbers of teams, which is expected since the numbers of variables and constraints scale with the number of teams. Additionally, the SWAP depth is typically larger in solutions with more teams since conflicts between teams are more frequent and there is less sharing of target destinations among qubits.

V. DISCUSSION

In this study, we explored the challenge of enhancing parts of the compilation process for quantum algorithms, focusing particularly on the multi-qubit pathfinding (MQPF) problem. We benchmarked compilation solutions across various hardware layouts and introduced a classical MQPF algorithm that navigates logical qubits grouped into teams on a quantum hardware layout towards designated target locations. The algorithm aims to minimise the number of

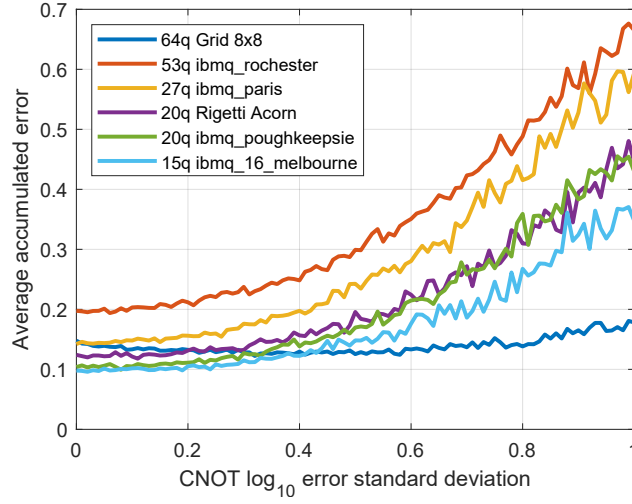


FIG. 9. Average accumulated error for pathfinding random instances of 10 logical qubits with random CNOT error rates for increasing variance for physical device layouts shown in Figure 1. Each data point is averaged over 100 random problem instances with CNOT errors sampled from truncated normal distributions on a log scale with a mean of 0.001 and specified \log_{10} error standard deviations. The \log_{10} standard deviations range from 0 to 1 increasing in increments of 0.01. Problem instances that exceed 1000 seconds are considered timed out and are ignored in the results. A \log_{10} standard deviation of 1 corresponds to 1 order of magnitude.

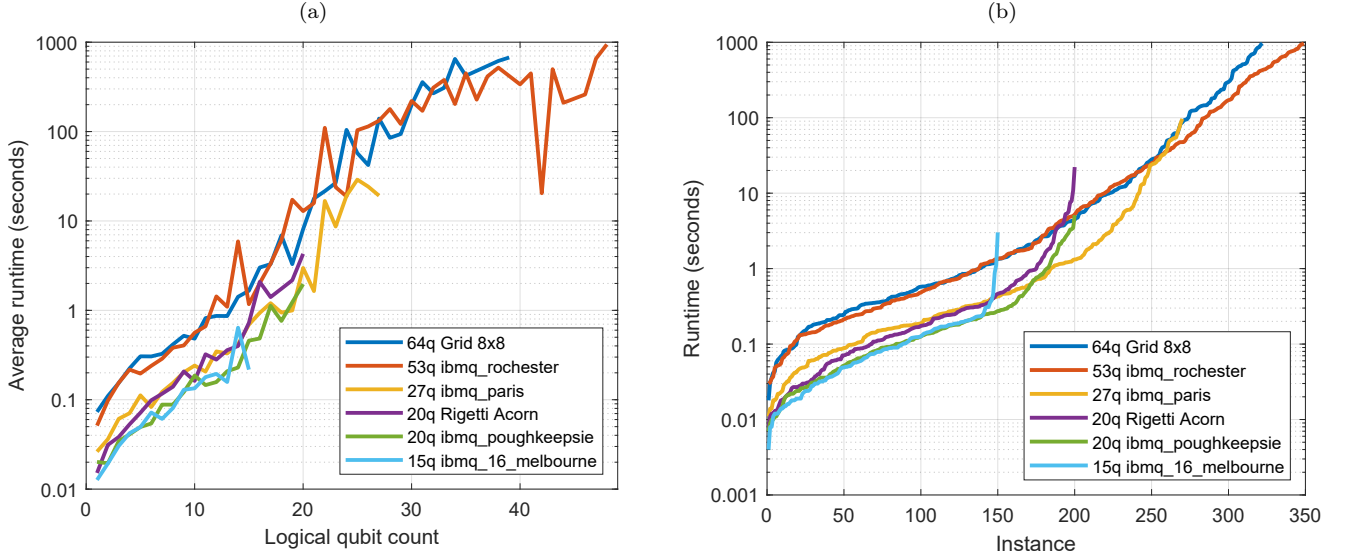


FIG. 10. Algorithm computational runtimes for multi-qubit pathfinding logical qubits on physical device layouts shown in Figure 1. There are 10 random instances for each number of logical qubits. Each logical qubit is in its own team. Problem instances that exceed 1000 seconds are considered timed out and are ignored, with the number of instances timed out for each number of logical qubits shown in Figure 6. The runtimes scale with the number of variables and constraints in the binary integer linear program generated for the solutions. (a) The average runtime for each number of logical qubits. (b) The runtimes for all instances sorted in ascending order.

time steps required, where each logical qubit can either remain idle, or swap with an adjacent qubit at each step. As a secondary objective, the algorithm minimises the total accumulated SWAP gate error rate in the resulting MQPF quantum circuit.

The MQPF algorithm, adapted from the binary integer linear program (BILP) formulation of the multi-commodity flow problem, models logical qubit navigation as a time-expanded graph. Each time step is represented as a layer comprising all nodes in the hardware graph. The edges between these layers denote possible movements between nodes in the hardware graph. The logical qubits navigate from the initial layer to the final layer by converting

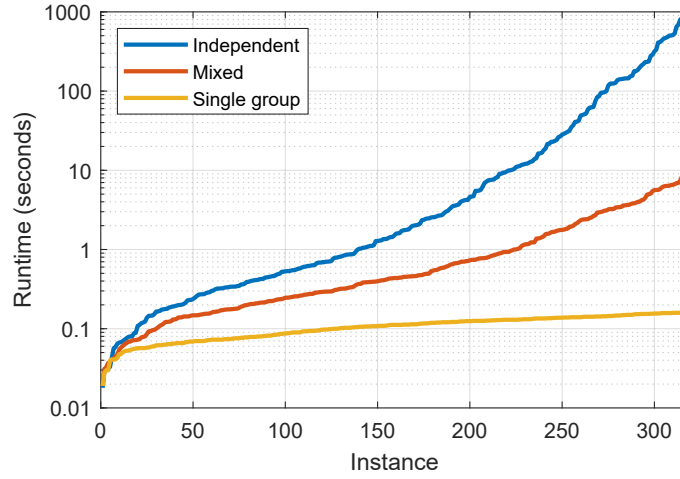


FIG. 11. The computational runtimes for three methods of assigning logical qubits to teams on the 64-qubit 8x8 grid hardware graph. The three methods used were: independent, where each logical qubit is in its own team; mixed, where logical qubits are randomly assigned to a random number of teams; and single group, where all logical qubits are in a single team. There are 10 random instances for each number of logical qubits from 1 to 64. Instances are sorted in ascending order of runtime.

the time-expanded graph into a BILP, which is solved using a mathematical programming solver. The number of layers increases until a valid solution is found, determining the optimal SWAP depth for the MQPF instance. The optimisation’s objective function corresponds to the accumulated SWAP gate error in the solution quantum circuits.

When applied to various quantum hardware layouts, the algorithm demonstrated that solutions for the 64-qubit grid layout had significantly lower SWAP depths than those for the 53-qubit heavy-hexagon IBM Quantum layout, despite the grid’s larger size and higher number of qubits. This is likely due to the grid’s higher connectivity, with nodes of degree 3 and 4, compared to the heavy-hexagon graph’s nodes of degree 2 and 3. The higher connectivity allows more direct paths to destinations for each qubit. Additionally, the 64-qubit grid exhibited lower accumulated error rates than all other layouts except the 15-qubit *ibmq_melbourne* device, another grid layout. This observation was initially surprising, considering the expected longer distances between initial and destination locations on larger layouts. However, the increased connectivity likely offers more directional options for logical qubits to move towards at every location, helping to avoid congestion and circumvent problematic CNOT gates with relatively high error rates. Regarding computational runtime, we found that larger devices are more time-consuming to compute for because the number of variables and constraints is higher. Although, we found that the 64-qubit grid’s runtime is similar to that of the 53-qubit heavy-hexagon layout, even though it is larger. This is likely due to lower SWAP depth solutions, resulting in a shallower time-expanded graph and reduced numbers of variables and constraints.

The advantages of the grid layout over the heavy-hexagon layout could advocate for favouring Google grid-like architectures [63, 64] over IBM heavy-hexagon architectures. However, Google devices are typically subjected to a crosstalk constraint, which prohibits adjacent qubits from participating in different operations simultaneously [16]. This constraint could significantly increase optimal SWAP depths, a question worth exploring in future research by modifying the BILP to include a crosstalk constraint.

State-of-the-art methods for solving the MQPF problem for optimal SWAP depth with multiple teams are often based on propositional satisfiability (SAT) [22, 23]. Our method’s computational runtime appears comparable, while further optimising for accumulated gate errors, though a detailed comparison would require analysis across a diverse set of problem instances and consider factors like specific solvers used, code implementation, and computational hardware. Leveraging state-of-the-art ILP solvers and approximation techniques, our approach provides a possible trade-off between optimality and computation time. Potential optimisations in the ILP solver could include column generation and Lagrangian relaxation techniques for multi-commodity flow [65], given many solution edges exhibit zero flow, indicating room for potential efficiency improvements. Additionally, our method offers flexibility in adapting the model to various mapping problems, such as managing higher numbers of destination nodes than source nodes and handling shared target destinations by different teams.

As a direction for future research, it would be interesting to explore extending this approach to encompass more aspects of general quantum circuit mapping. This could include integrating the qubit allocation problem, where the focus shifts from destination constraints to constraints based on logical-qubit interactions.

ACKNOWLEDGEMENTS

The author would like to thank Sarama Tonetto, Michael Jones, Charles Hill, and Lloyd Hollenberg for valuable discussions and feedback. This work was supported by the University of Melbourne through the establishment of an IBM Quantum Network Hub at the University. This work was supported by an Australian Government Research Training Program Scholarship.

DATA AVAILABILITY STATEMENT

The code and datasets used in the current study are available at doi.org/10.5281/zenodo.11379442.

-
- [1] Dmitri Maslov, Sean M Falconer, and Michele Mosca. Quantum circuit placement. *IEEE Transactions on Computer-Aided Design of Integrated Circuits and Systems*, 27(4):752–763, 2008.
 - [2] Adi Botea, Akihiro Kishimoto, and Radu Marinescu. On the complexity of quantum circuit compilation. In *Eleventh Annual Symposium on Combinatorial Search*, 2018.
 - [3] He-Liang Huang, Xiao-Yue Xu, Chu Guo, Guojing Tian, Shi-Jie Wei, Xiaoming Sun, Wan-Su Bao, and Gui-Lu Long. Near-term quantum computing techniques: Variational quantum algorithms, error mitigation, circuit compilation, benchmarking and classical simulation. *Science China Physics, Mechanics & Astronomy*, 66(5):250302, 2023.
 - [4] Janusz Kusyk, Samah M Saeed, and Muharrem Umit Uyar. Survey on quantum circuit compilation for noisy intermediate-scale quantum computers: Artificial intelligence to heuristics. *IEEE Transactions on Quantum Engineering*, 2:1–16, 2021.
 - [5] Debjyoti Bhattacharjee and Anupam Chattopadhyay. Depth-optimal quantum circuit placement for arbitrary topologies. *arXiv preprint arXiv:1703.08540*, 2017.
 - [6] Chi Zhang, Ari B Hayes, Longfei Qiu, Yuwei Jin, Yanhao Chen, and Eddy Z Zhang. Time-optimal qubit mapping. In *Proceedings of the 26th ACM International Conference on Architectural Support for Programming Languages and Operating Systems*, pages 360–374, 2021.
 - [7] Gushu Li, Yufei Ding, and Yuan Xie. Tackling the qubit mapping problem for NISQ-era quantum devices. In *Proceedings of the Twenty-Fourth International Conference on Architectural Support for Programming Languages and Operating Systems*, pages 1001–1014, 2019.
 - [8] Alwin Zulehner, Alexandru Paler, and Robert Wille. An efficient methodology for mapping quantum circuits to the IBM QX architectures. *IEEE Transactions on Computer-Aided Design of Integrated Circuits and Systems*, 38(7):1226–1236, 2018.
 - [9] Angelo Oddi and Riccardo Rasconi. Greedy randomized search for scalable compilation of quantum circuits. In *Integration of Constraint Programming, Artificial Intelligence, and Operations Research: 15th International Conference, CPAIOR 2018, Delft, The Netherlands, June 26–29, 2018, Proceedings 15*, pages 446–461. Springer, 2018.
 - [10] Bochen Tan and Jason Cong. Optimal layout synthesis for quantum computing. In *Proceedings of the 39th International Conference on Computer-Aided Design*, pages 1–9, 2020.
 - [11] Robert Wille, Lukas Burgholzer, and Alwin Zulehner. Mapping quantum circuits to IBM QX architectures using the minimal number of SWAP and H operations. In *Proceedings of the 56th Annual Design Automation Conference 2019*, pages 1–6, 2019.
 - [12] Robert Wille, Aaron Lye, and Rolf Drechsler. Optimal SWAP gate insertion for nearest neighbor quantum circuits. In *2014 19th Asia and South Pacific Design Automation Conference (ASP-DAC)*, pages 489–494. IEEE, 2014.
 - [13] Beatrice Nash, Vlad Gheorghiu, and Michele Mosca. Quantum circuit optimizations for NISQ architectures. *Quantum Science and Technology*, 5(2):025010, 2020.
 - [14] Yangzhi Li, Wen Liu, Maoduo Li, and Yugang Li. Quantum circuit compilation for nearest-neighbor architecture based on reinforcement learning. *Quantum Information Processing*, 22(8):295, 2023.
 - [15] Yuwei Jin, Jason Luo, Lucent Fong, Yanhao Chen, Ari B Hayes, Chi Zhang, Fei Hua, and Eddy Z Zhang. A structured method for compilation of QAOA circuits in quantum computing. *arXiv preprint arXiv:2112.06143*, 2021.
 - [16] Kyle Booth, Minh Do, J Beck, Eleanor Rieffel, Davide Venturelli, and Jeremy Frank. Comparing and integrating constraint programming and temporal planning for quantum circuit compilation. In *Proceedings of the International Conference on Automated Planning and Scheduling*, volume 28, 2018.
 - [17] Davide Venturelli, Minh Do, Eleanor Rieffel, and Jeremy Frank. Compiling quantum circuits to realistic hardware architectures using temporal planners. *Quantum Science and Technology*, 3(2):025004, 2018.
 - [18] Davide Venturelli, Minh Do, Eleanor Gilbert Rieffel, and Jeremy Frank. Temporal planning for compilation of quantum approximate optimization circuits. In *IJCAI*, pages 4440–4446, 2017.
 - [19] Marcos Yukio Siraichi, Vinícius Fernandes dos Santos, Caroline Collange, and Fernando Magno Quintão Pereira. Qubit allocation as a combination of subgraph isomorphism and token swapping. *Proceedings of the ACM on Programming Languages*, 3(OOPSLA):1–29, 2019.

- [20] Pengcheng Zhu, Xueyun Cheng, and Zhijin Guan. An exact qubit allocation approach for NISQ architectures. *Quantum Information Processing*, 19(11):391, 2020.
- [21] Alireza Shafaei, Mehdi Saeedi, and Massoud Pedram. Qubit placement to minimize communication overhead in 2D quantum architectures. In *2014 19th Asia and South Pacific Design Automation Conference (ASP-DAC)*, pages 495–500. IEEE, 2014.
- [22] Pavel Surynek. Multi-agent path finding with generalized conflicts: An experimental study. In *International Conference on Agents and Artificial Intelligence*, pages 118–142. Springer, 2019.
- [23] Pavel Surynek. Conflict handling framework in generalized multi-agent path finding: Advantages and shortcomings of satisfiability modulo approach. In *ICAART (2)*, pages 192–203, 2019.
- [24] Aaron Lye, Robert Wille, and Rolf Drechsler. Determining the minimal number of swap gates for multi-dimensional nearest neighbor quantum circuits. In *The 20th Asia and South Pacific Design Automation Conference*, pages 178–183. IEEE, 2015.
- [25] Alexandru Paler, Alwin Zulehner, and Robert Wille. Nisq circuit compilation is the travelling salesman problem on a torus. *Quantum Science and Technology*, 6(2):025016, 2021.
- [26] IBM Quantum Platform. <https://www.ibm.com/quantum>. (Accessed 15 May 2024).
- [27] JS Otterbach, R Manenti, N Alidoust, A Bestwick, M Block, B Bloom, S Caldwell, N Didier, E Schuyler Fried, S Hong, et al. Unsupervised machine learning on a hybrid quantum computer. *arXiv preprint arXiv:1712.05771*, 2017.
- [28] Ravindran Kannan and Clyde L Monma. On the computational complexity of integer programming problems. In *Optimization and Operations Research*, pages 161–172. Springer, 1978.
- [29] Thomas S Ferguson et al. Who solved the secretary problem? *Statistical Science*, 4(3):282–289, 1989.
- [30] Michele Conforti, Gérard Cornuéjols, Giacomo Zambelli, et al. *Integer programming*, volume 271. Springer, 2014.
- [31] Robert J Vanderbei et al. *Linear programming*, volume 3. Springer, 2015.
- [32] Xiaocheng Li, Chunlin Sun, and Yinyu Ye. Simple and fast algorithm for binary integer and online linear programming. *arXiv preprint arXiv:2003.02513*, 2020.
- [33] Ellis L Johnson, George L Nemhauser, and Martin WP Savelsbergh. Progress in linear programming-based algorithms for integer programming: An exposition. *Inform Journal on Computing*, 12(1):2–23, 2000.
- [34] Dag Wedelin. An algorithm for large scale 0–1 integer programming with application to airline crew scheduling. *Annals of Operations Research*, 57(1):283–301, 1995.
- [35] Peter E Hart, Nils J Nilsson, and Bertram Raphael. A formal basis for the heuristic determination of minimum cost paths. *IEEE Transactions on Systems Science and Cybernetics*, 4(2):100–107, 1968.
- [36] Hang Ma and Sven Koenig. Optimal target assignment and path finding for teams of agents. *arXiv preprint arXiv:1612.05693*, 2016.
- [37] Jingjin Yu and Steven M LaValle. Multi-agent path planning and network flow. In *Algorithmic Foundations of Robotics X*, pages 157–173. Springer, 2013.
- [38] Jack Edmonds and Richard M Karp. Theoretical improvements in algorithmic efficiency for network flow problems. *Journal of the ACM (JACM)*, 19(2):248–264, 1972.
- [39] Ko-Hsin Cindy Wang, Adi Botea, et al. Fast and memory-efficient multi-agent pathfinding. In *ICAPS*, pages 380–387, 2008.
- [40] Lydia E Kavraki, Petr Svestka, J-C Latombe, and Mark H Overmars. Probabilistic roadmaps for path planning in high-dimensional configuration spaces. *IEEE Transactions on Robotics and Automation*, 12(4):566–580, 1996.
- [41] Ryan Luna and Kostas E Bekris. Network-guided multi-robot path planning in discrete representations. In *2010 IEEE/RSJ International Conference on Intelligent Robots and Systems*, pages 4596–4602. IEEE, 2010.
- [42] Francesco Basile, Pasquale Chiacchio, and Jolanda Coppola. A hybrid model of complex automated warehouse systems—Part I: Modeling and simulation. *IEEE Transactions on Automation Science and Engineering*, 9(4):640–653, 2012.
- [43] Jingjin Yu and Steven M LaValle. Planning optimal paths for multiple robots on graphs. In *2013 IEEE International Conference on Robotics and Automation*, pages 3612–3617. IEEE, 2013.
- [44] Pavel Surynek. Reduced time-expansion graphs and goal decomposition for solving cooperative path finding sub-optimally. In *IJCAI*, pages 1916–1922, 2015.
- [45] Esra Erdem, Doga Kisa, Umut Oztok, and Peter Schüller. A general formal framework for pathfinding problems with multiple agents. In *Proceedings of the AAAI Conference on Artificial Intelligence*, volume 27, 2013.
- [46] Trevor Standley. Finding optimal solutions to cooperative pathfinding problems. In *Proceedings of the AAAI Conference on Artificial Intelligence*, volume 24, 2010.
- [47] Guni Sharon, Roni Stern, Meir Goldenberg, and Ariel Felner. The increasing cost tree search for optimal multi-agent pathfinding. *Artificial Intelligence*, 195:470–495, 2013.
- [48] Liron Cohen, Tansel Uras, and Sven Koenig. Feasibility study: Using highways for bounded-suboptimal multi-agent path finding. In *Eighth Annual Symposium on Combinatorial Search*, 2015.
- [49] Guni Sharon, Roni Stern, Ariel Felner, and Nathan R Sturtevant. Conflict-based search for optimal multi-agent pathfinding. *Artificial Intelligence*, 219:40–66, 2015.
- [50] Eli Boyarski, Ariel Felner, Roni Stern, Guni Sharon, Oded Betzalel, David Tolpin, and Eyal Shimony. ICBS: The improved conflict-based search algorithm for multi-agent pathfinding. In *Eighth Annual Symposium on Combinatorial Search*. Citeseer, 2015.
- [51] Van Nguyen, Philipp Obermeier, Tran Cao Son, Torsten Schaub, and William Yeoh. Generalized target assignment and path finding using answer set programming. In *Twelfth Annual Symposium on Combinatorial Search*, 2019.

- [52] Wolfgang Hönig, Scott Kiesel, Andrew Tinka, Joseph Durham, and Nora Ayanian. Conflict-based search with optimal task assignment. In *Proceedings of the International Joint Conference on Autonomous Agents and Multiagent Systems*, 2018.
- [53] Noga Alon, Fan RK Chung, and Ronald L Graham. Routing permutations on graphs via matchings. *SIAM Journal on Discrete Mathematics*, 7(3):513–530, 1994.
- [54] Katsuhisa Yamanaka, Erik D Demaine, Takehiro Ito, Jun Kawahara, Masashi Kiyomi, Yoshio Okamoto, Toshiki Saitoh, Akira Suzuki, Kei Uchizawa, and Takeaki Uno. Swapping labeled tokens on graphs. *Theoretical Computer Science*, 586: 81–94, 2015.
- [55] Jun Kawahara, Toshiki Saitoh, and Ryo Yoshinaka. The time complexity of the token swapping problem and its parallel variants. In *International Workshop on Algorithms and Computation*, pages 448–459. Springer, 2017.
- [56] Tillmann Miltzow, Lothar Narins, Yoshio Okamoto, Günter Rote, Antonis Thomas, and Takeaki Uno. Approximation and hardness for token swapping. *arXiv preprint arXiv:1602.05150*, 2016.
- [57] Édouard Bonnet, Tillmann Miltzow, and Paweł Rżazewski. Complexity of token swapping and its variants. *Algorithmica*, 80(9):2656–2682, 2018.
- [58] Mark R Jerrum. The complexity of finding minimum-length generator sequences. *Theoretical Computer Science*, 36: 265–289, 1985.
- [59] Arthur Cayley. LXXVII. Note on the theory of permutations. *The London, Edinburgh, and Dublin Philosophical Magazine and Journal of Science*, 34(232):527–529, 1849.
- [60] Katsuhisa Yamanaka, Takashi Horiyama, David Kirkpatrick, Yota Otachi, Toshiki Saitoh, Ryuhei Uehara, and Yushi Uno. Computational complexity of colored token swapping problem. *IPSI SIG Technical Report*, 156(2), 2016.
- [61] Philippe Mahey, Adam Ouorou, Larry Leblanc, and Jerome Chifflet. A new proximal decomposition algorithm for routing in telecommunication networks. *Networks: An International Journal*, 31(4):227–238, 1998.
- [62] Gurobi Optimization LLC. Gurobi optimizer reference manual. <http://www.gurobi.com>, 2021.
- [63] Sergio Boixo, Sergei V Isakov, Vadim N Smelyanskiy, Ryan Babbush, Nan Ding, Zhang Jiang, Michael J Bremner, John M Martinis, and Hartmut Neven. Characterizing quantum supremacy in near-term devices. *Nature Physics*, 14(6):595–600, 2018.
- [64] Frank Arute, Kunal Arya, Ryan Babbush, Dave Bacon, Joseph C Bardin, Rami Barends, Rupak Biswas, Sergio Boixo, Fernando GSL Brandao, David A Buell, et al. Quantum supremacy using a programmable superconducting processor. *Nature*, 574(7779):505–510, 2019.
- [65] DAI Weibin, Jun Zhang, and SUN Xiaoqian. On solving multi-commodity flow problems: An experimental evaluation. *Chinese Journal of Aeronautics*, 30(4):1481–1492, 2017.